ACS APPLIED MATERIALS & INTERFACES

Research Article

www.acsami.org

Synthesis and Characterization of Gold/Alanine Nanocomposites with Potential Properties for Medical Application as Radiation Sensors

Eder José Guidelli,*[,†] Ana Paula Ramos,[‡] Maria Elisabete D. Zaniquelli,[‡] Patricia Nicolucci, and Oswaldo Baffa[†]

[†]Departamento de Física and [‡]Departamento de Química, Faculdade de Filosofia, Ciências e Letras de Ribeirão Preto, Universidade de São Paulo, Avenida Bandeirantes 3900, 14040-901 Ribeirão Preto, São Paulo, Brazil

ABSTRACT: Radiation dose assessment is essential for several medical treatments and diagnostic procedures. In this context, nanotechnology has been used in the development of improved radiation sensors, with higher sensitivity as well as smaller sizes and energy dependence. This paper deals with the synthesis and characterization of gold/alanine nanocomposites with varying mass percentage of gold, for application as radiation sensors. Alanine is an excellent stabilizing agent for gold nanoparticles because the size of the nanoparticles does not augment with increasing mass percentage of gold, as evidenced by UV−vis spectroscopy, dynamic light scattering, and transmission electron microscopy. X-ray diffraction patterns suggest that the alanine crystalline orientation undergoes alterations upon the addition of gold nanoparticles. Fourier transform infrared spectroscopy indicates that there is interaction between the gold nanoparticles and the amine group of the alanine molecules, which may be the reason for the enhanced stability of the nanocomposite. The application of the nanocomposites as radiation detectors was evaluated by the electron spin resonance technique. The sensitivity is improved almost 3 times in the case of the nanocomposite containing 3% (w/w) gold, so it can be easily tuned by changing the amount of gold nanoparticles in the nanocomposites, without the size of the nanoparticles influencing the radiation absorption. In conclusion, the featured properties, such as homogeneity, nanoparticle size stability, and enhanced sensitivity, make these nanocomposites potential candidates for the construction of small-sized radiation sensors with tunable sensitivity for application in several medical procedures.

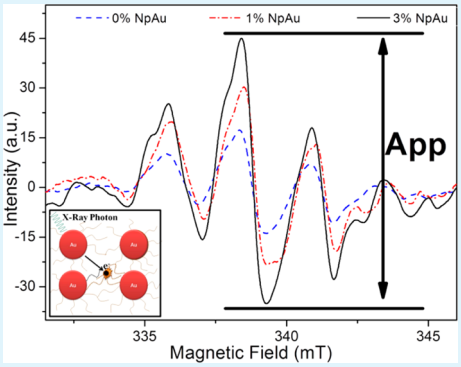

KEYWORDS: *radiation sensor, nanoparticles, gold, alanine, ESR, EPR*

1. INTRODUCTION

Ionizing radiation is largely employed in the industrial and medical areas. This makes radiation dose assessment essential for medical treatment and diagnosis, such as cancer radiation therapy,[1,2] tomography, radiography,[3,4] and fluoroscopy,[5] as well as for radiological protection[6] and personal dosimetry.[7] Therefore, the development of adequate radiation sensors that comply with each specific application is of utmost importance. The most common sensors utilized for radiation measurements are ionization chambers,[8] scintillation detectors, thermoluminescent and optically stimulated luminescent dosimeters,[9,10] and semiconductor devices.[11] Electron spin resonance (ESR) spectroscopy also plays an important role in the field of radiation detection when it comes to the identification and quantification of radiation-induced free radicals in materials.[12−14] Among a variety of compounds used for radiation detection by means of the ESR technique, alanine stands out.[15−17]

Nowadays, the alanine/ESR technique is largely employed for dosimetry of high doses involved in procedures of food irradiation, medical product sterilization, and radiotherapy.[18−20] This technique can detect doses from gray up to kilogray and offers such advantages as time stability of the ESR signal and linearity.[16] The stability of the radicals depends on the molecular surroundings, rigidity of the matter, temperature, and humidity.[16] It is worth noting that alanine is a tissue-equivalent biomaterial; i.e., its effective atomic number is close to that of soft tissues, so it absorbs the ionizing radiation in a way similar to that of tissues.[16] However, alanine has its sensitivity diminished for low doses and low-energy photons (energy below 100 keV).[16,21] The sensitivity reduction reaches values up to 40% for X-ray beams with energy below 100 keV, compared with ^{60}Co irradiations.[16]

Besides the low sensitivity for low energy and doses, the dosimetry of narrow photon beams, such as the ones employed in radiosurgery and intensity-modulated radiation therapy of cancer, requires utilization of small-sized radiation detectors, so that the required spatial resolution is achieved.[22,23] However, reducing the size of the alanine radiation detectors lowers their

Received: July 27, 2012
Accepted: October 15, 2012
Published: October 15, 2012

   dx.doi.org/10.1021/am3014899 | *ACS Appl. Mater. Interfaces* 2012, 4, 5844−5851

sensitivity because the latter depends on the amount of free radicals produced by the radiation.[1]

In this sense, many efforts have been made toward the development of improved radiation sensors that can be used for a wide range of applications. Some properties of the sensing materials have been modified, enhancing the sensor performance. To this end, a standard method employed for improving the sensitivity of radiation detectors is the use of composites for which the matrix is composed of the sensing material and the reinforcement consists of a high atomic number material, which raises absorption of the radiation.[21,24−28] However, this gain in sensitivity implies reduced tissue equivalence.[21,26] Moreover, for the construction of small radiation detectors, the inhomogeneity of the composite can significantly decrease the sensitive volume of the detector, thus implying in a wrong dose assessment.[29]

In this context, nanotechnology can produce composites containing stable nanoparticles with controlled size,[30,31] for application as radiation sensors.[32−34] Once again, alanine stands out. At the same time that it is suitable for radiation detection, it can be utilized as a reducing, capping, and stabilizing agent for the production of silver nanoparticles. The silver/alanine nanocomposites display increased sensitivity and reduced energy dependence compared to pure DL-alanine. The enhancement in the radiation detection sensitivity is due to the presence of silver nanoparticles, which is attributed to the electrons ejected by the metal upon its interaction with the ionizing radiation, culminating in dose delivery to the detecting material.[21,24,25,35,36] However, it has been noticed that the rise in the mass percentage of silver in silver/alanine nanocomposites causes instability and augments the size of the nanoparticles, what is accompanied by a reduction in the sensitivity of the detectors.[29] This is the reason why we have chosen to employ gold nanoparticles.

In fact, it has been reported that the dose deposition around nanoparticles depends on their size.[37] An increase in the size of gold nanoparticles from 2 to 100 nm has revealed that, in the case of the larger particles, more than 30% of the energy of the secondary electrons is self-absorbed by the nanoparticles.[37] Because the dose that is absorbed by the nanoparticles does not contribute to the production of radiation-induced free radicals, it diminishes the sensitivity of the alanine composites employed as radiation detectors.[29] This emphasizes that the production of nanoparticles as small as possible is important for the reduction of the portion of energy that is self-absorbed, thereby enhancing and optimizing the sensitivity of such radiation sensors. The synthesis of homogeneous composites for application as radiation sensors is crucial in order to ensure dose assessment reliability.

This paper reports on the production of alanine composites containing 5 ± 2 nm gold nanoparticles, for application as radiation sensors in medical procedures. The synthesis is facile and rapid and occurs at room temperature. The morphological and structural properties of the nanocomposites with varying amounts of gold nanoparticles, as well as stabilization of the gold nanoparticles by alanine, are explored. The application of the nanocomposites as radiation sensors was evaluated by ESR spectroscopy. These nanocomposites have featured properties, such as homogeneity, nanoparticle size stability, and enhanced sensitivity, that enable the construction of small-sized radiation sensors for use in a variety of medical procedures.

2. MATERIALS AND METHODS

The chemicals employed in the experiments were of analytical reagent grade and were used as received. Chloroauric acid ($HAuCl_4$; 99.999%) was provided by Sigma-Aldrich, sodium borohydride ($NaBH_4$) was purchased from Vetec (Brazil), and DL-alanine (99%) was obtained from Acros Organics. The only difference between L-alanine and DL-alanine is that L-alanine is more sensitive than DL-alanine, but otherwise the conclusions draw with the use of this isomeric mix will be valid for the L isomer. Milli-Q water was used to prepare all of the aqueous solutions. Gold nanoparticles were synthesized by means of the chemical reduction of the gold salt as follows: A 2 mmol L^{-1} $HAuCl_4$ aqueous solution was added to a freshly prepared 8 mmol L^{-1} $NaBH_4$ aqueous solution, under vigorous stirring. The color of the system changed from yellow to red, indicating the formation of a colloidal gold dispersion. The system was kept under stirring for 12 h, in order to guarantee total gold-ion reduction. Gold nanoparticle formation was confirmed by the plasmonic absorption peak at 515 nm present in the UV−vis spectrum. Dynamic light scattering (DLS) technique measurements indicated that gold nanoparticles had a mean size of 5 ± 2 nm. The sol was stable, with no breaking down of the colloid within a period of about 1 month. Thereafter, different volumes of 1.1 mol L^{-1} alanine aqueous solution were added to the gold nanoparticle dispersion. The gold mass percentage in the nanocomposites was varied from 0.01% up to 3%. The dispersions were dried in an oven at a temperature of 40 °C, yielding the powdered nanocomposites. The samples were named according to the mass percentage of gold present in the dried nanocomposites (Table 1). For example, the nanocomposite prepared with Au^+ 0.01% (w/w) was named 0.01%NpAu and so on, up to the sample 3%NpAu.

Table 1. Mass Percentage of the Components Present in Each Sample and Its Respective Sample Name

DL-alanine (% mass)	NpAu (% mass)	sample name
100.0	0.00	0%NpAu
99.99	0.01	0.01%NpAu
99.90	0.10	0.1%NpAu
99.50	0.50	0.5%NpAu
99.00	1.00	1%NpAu
97.00	3.00	3%NpAu

The UV−vis absorption spectra of the colloidal dispersions were acquired on an Ultrospec 2100 pro (Amersham Pharmacia) spectrophotometer. The particle size distribution was acquired by the DLS technique, using a Zeta-Sizer system (Malvern Instruments), at a fixed wavelength and angle (633 nm He−Ne laser, 90°). The X-ray diffraction (XRD) patterns of the powder samples were recorded on a Siemens D5005 diffractometer, over the range $20° \leq 2\theta \leq 80°$, with an increment of 0.02°. The Cu Kα emission line (1.541 Å, 40 kV, and 40 mA) coupled to a graphite monochromator was employed. Nanoparticle morphology and size were examined by means of a JEOL JEM-100 CXII transmission electron microscope by drying a drop of the colloidal dispersions on a copper grid covered with a conductive polymer. Fourier transform infrared (FTIR) spectra were registered on a Bomem MB 100 spectrometer using a KBr pellet, in the region between 4000 and 40 cm^{-1}.

The aim of this work was to investigate the influence of gold nanoparticles on the structural and dosimetric properties of the nanocomposites. Once the influence of high-atomic-number materials is more relevant for low-energy photons, the powdered nanocomposites were irradiated on a Siemens Stabilipan II clinical orthovoltage with an effective energy of 90 keV and a dose of 5 Gy. To irradiate the samples, approximately 30 mg powder samples were placed in cylindrical capsules with dimensions of 1.0 × 0.5 cm, which, in turn, were placed over a 10 cm acrylic layer as the backscatter medium, without a buildup cap. A 1.28 mm copper filter was employed, and the kVp was 180 kV. The source-to-dosimeter distance

was 40 cm, and the field size was 8 × 10 cm^2. These procedures were carried out at the Radiotherapy Service of HC-FMRP-USP.

In order to construct the dose response curve, the samples were irradiated from 1 Gy up to 50 Gy at the Department of Physics, FFCLRP-USP. The X-ray source was an industrial X-ray tube (Philips PW 2215/20) with a stationary molybdenum target, adapted with an aluminum filter, and attached to a constant-potential generator (Phillips PANalytical PW 3830). The tube operates at 35 kVp and 30 mA. The X-ray spectrum was published elsewhere.[38] These irradiations were performed in air, with a 50 cm source-to-dosimeter distance, and at room temperature.

The ESR spectra of the irradiated samples were accomplished on a JEOL JES-FA 200 (9.5 GHz) spectrometer. To this end, approximately 30 mg samples were placed in quartz tubes, which were positioned in the center of the standard JEOL cylindrical cavity. This procedure guarantees that the whole sample is inside the active volume of the ESR cavity. The ESR parameters employed for the measurements were fixed as follows: room temperature, central field at 338.5 mT, microwave power = 5mW, sweep time = 1 min, sweep width = 10 mT, modulation amplitude = 0.4 mT, magnification = 3000×, and time constant = 0.3 s. Five scans were taken for each sample. Routine measurements of the Mn^{2+} standard are performed to correct for possible response variations in the spectrometer from day to day.

In order to compare the signal amplitudes of the different samples, the spectrum of each nanocomposite was normalized by the total mass of its respective sample (mass of alanine + mass of gold nanoparticles).

3. RESULTS AND DISCUSSION

The UV−vis spectra of the colloidal gold dispersions are depicted in Figure 1. The absorption peak at 515 nm is

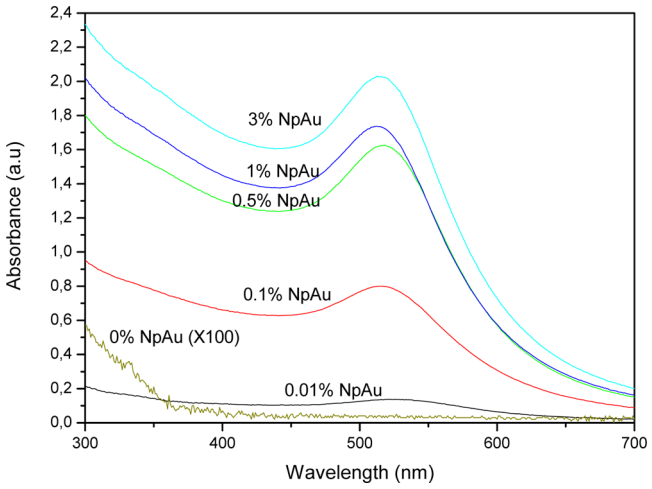

Figure 1. UV−vis spectra of the colloidal gold dispersion.

characteristic of spherical gold nanoparticles[39,40] and is related to the collective oscillation of the free electrons at the nanoparticles surface, giving rise to the so-called plasmonic absorption peak. The position of the peak is related to the particle size, and the full width at half-maximum (fwhm) is associated with the nanoparticle size distribution.[41] The position of the plasmonic peak is not shifted, and the fwhm remains constant as the gold nanoparticle concentration rises. This indicates that the system is composed of stable spherical particles that do not aggregate even at a high mass percentage of gold.

The particle size distributions obtained by the DLS technique for samples 0.01%NpAu and 1%NpAu are presented in Figure 2. These results agree with the UV−vis spectroscopy data, revealing that increasing gold mass percentage in the colloidal dispersion does not modify the nanoparticle size. In fact, some authors have shown that the quantity of the reducing/capping agent has a marked influence on the particle size distribution.[42,43] Our previous studies have evidenced that the elevation in the silver mass percentage in silver/alanine nanocomposites causes agglomeration and particle growth.[29] However, this is not the case for the gold/alanine nanocomposites described herein. One should be aware of the particle size differences between these two kinds of nanocomposites. Whereas for the silver nanocomposites the smallest size is 30 nm, gold nanocomposites have sizes as low as 5 nm. It is known that larger stability results can usually be explained by the diminished van der Waals attraction between small particles.[44] Nevertheless, despite the very small size of the gold nanoparticles, we were able to detect an additional stabilizing effect of alanine because these gold/alanine dispersions are stable even for a year. The ones without alanine are stable for only less than 1 month. Therefore, the colloidal stability and the practical absence of Ostwald ripening (particle size distribution constancy) suggest that the combined results of small size and stabilizing effect provided by alanine allows for the formation of very stable gold nanoparticles via mechanisms in which alanine participates in a reasonably complex manner.

The XRD patterns of the powdered samples 0%NpAu, 0.1% NpAu, 0.5% NpAu, 1% NpAu, and 3%NpAu are shown in Figure 3. The gold nanoparticles have crystalline structures with face-centered cubic phases, attributed to the presence of peaks related to planes with Miller indices (111), (200), (311), and (222).[45] Because the Debye−Scherer equation gives an approximation for the medium nanocrystallite size that is inversely proportional to the fwhm of diffractogram peaks, the broad aspect of these peaks confirms that small-sized nanoparticles are produced.[46]

The peaks related to the DL-alanine orthorhombic crystalline structure can also be observed. They are indexed as (210) sitting at 20.7°, (400) at 29.7°, (002) at 30.8°, (410) at 33.2°, and (112) at 34.9°.[29] The alanine crystallinity is measured as the area of each peak divided by the sum of all of the areas of the peaks related to the alanine orthorhombic crystalline structure. Figure 4a corresponds the alanine crystallinity measured by means of the (210) plane. The addition of 0.1% gold nanoparticles to the alanine matrix decreases the crystallinity by 6%. This reduction remains the same as the gold nanoparticle concentration is raised. In the opposite trend, the alanine crystallinity measured by means of all of the other peaks increases (Figure 4b). Thus, gold nanoparticle insertion in the alanine matrix seems to modify the amino acid crystalline orientation. This could be rationalized as follows: the presence of 0.1% small-sized nanoparticles may drive alanine crystallization in such a way that the colloidal gold is embedded in the alanine crystal, thereby causing crystallite disorder and diminishing the crystalline orientation along the (210) plane (Figure 4c). This change in orientation may also be due to a perturbation in the hydrogen bonding between the alanine amino acid groups responsible for the crystal formation.[47] However, 0.1% (w/w) seems to be a limit for gold particle insertion. An additional amount of gold nanoparticles cannot be accommodated inside the alanine matrix, perhaps for simple geometric reasons or due to energy considerations. Hence, the exceeding particles should be arranged outside the needlelike alanine crystals (Figure 4d). This suggests that gold nano-

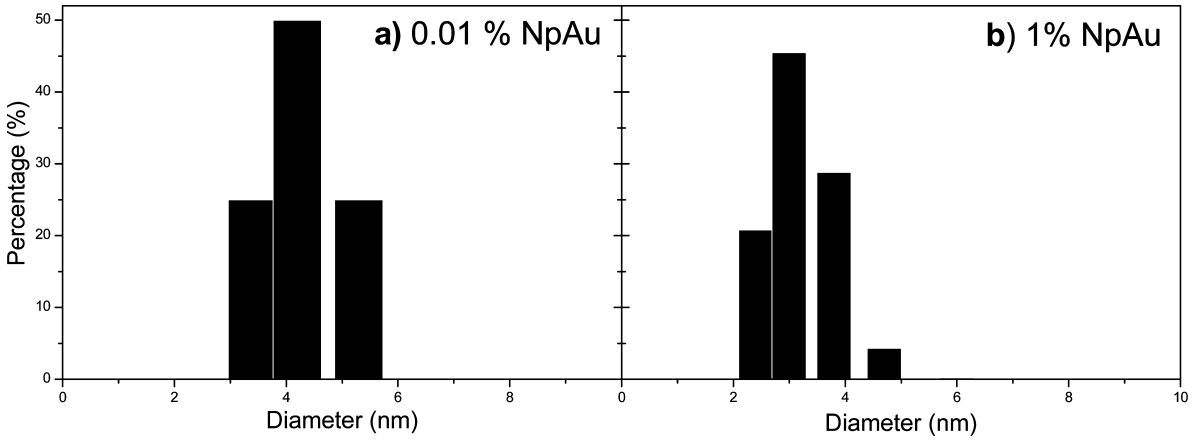

Figure 2. Particle size distributions of gold nanoparticles: (a) sample 0.1%NpAu; (b) sample 1%NpAu.

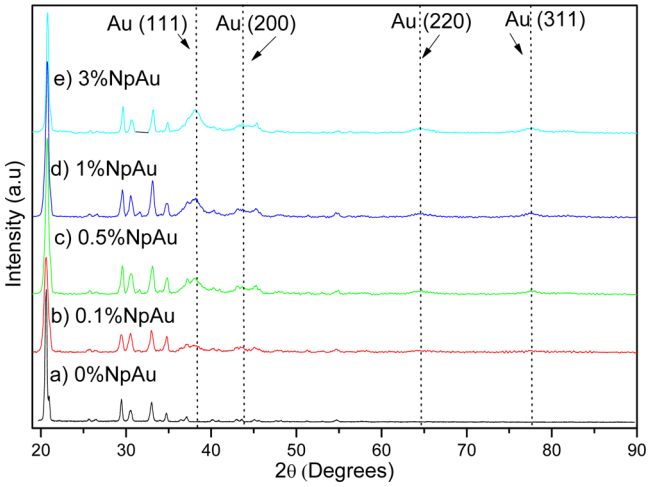

Figure 3. XRD patterns of gold/alanine nanocomposites.

particles may interact with DL-alanine molecules in two different ways, that is, by occupying internal and/or external positions in relation to the alanine crystal, depending on the employed gold/alanine mass percentage.

Similar results were also obtained in the case of silver/alanine nanocomposites, as published elsewhere.[29] Silver nanoparticle segregation in specific samples was attributed to the presence of large particles, thus evidencing that the nanoparticle size influences their position in the alanine matrix.[29] Here, it is worth noting that, although the average gold nanoparticle size remains constant upon varying gold concentration, particle segregation is also verified for samples with higher gold mass percentage. In the case of silver/alanine nanocomposites, there is total expulsion of the silver nanoparticles from the alanine matrix in the samples containing larger particles.[29] For gold/alanine nanocomposites, the gold nanoparticles still remain accommodated inside the alanine matrix, and only the exceeding gold nanoparticles are expelled from the alanine

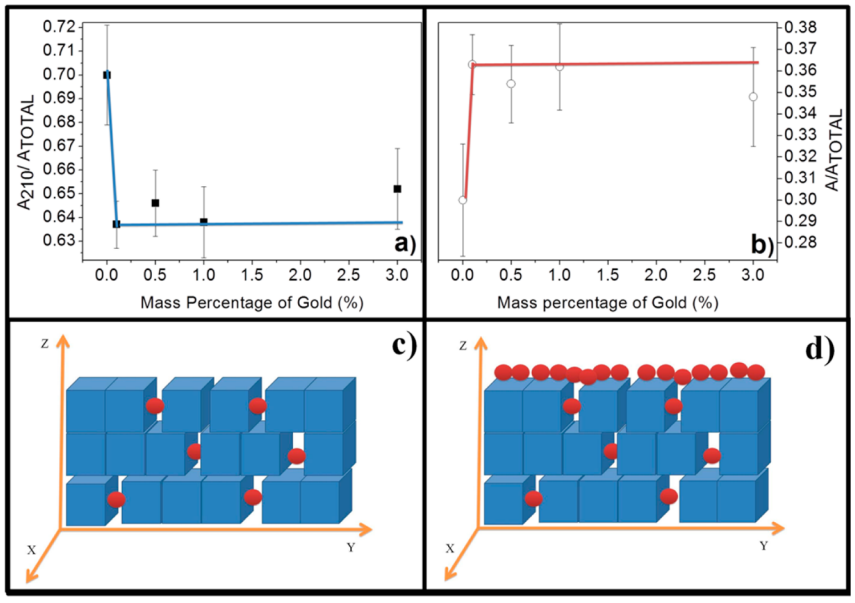

Figure 4. Crystallinity of DL-alanine as measured by the (210) plane (a) and by the sum of all other peaks (b). The crystallinity was measured as the area of each peak in the XRD pattern of DL-alanine divided by the total area of the peaks associated with the DL-alanine orthorhombic crystalline structure. (c) Presence of 0.1% of small-sized nanoparticles that drive the alanine crystallization in such way that the colloidal gold nanoparticles are embedded in the alanine crystal. (d) Additional amount of gold nanoparticles not accommodated inside the alanine matrix. Then, the exceeding particles are arranged outside the alanine crystals. These representative figures were adapted from ref 29.

dx.doi.org/10.1021/am3014899 | ACS Appl. Mater. Interfaces 2012, 4, 5844−5851

crystals. This suggests that the concentration is also relevant when it comes to the position of the nanoparticles in the alanine matrix.

In fact, the addition of arginine-capped gold nanoparticles to a L-alanine matrix has already been investigated, showing that the former favor the L-alanine crystalline orientation preferentially along the *c* axes.[48] This is ascribed to arginine adsorption onto faces (120) and (011) during L-alanine crystal growth. Because the gold nanoparticles employed in our experiments were not capped by any stabilizing agent, we believe that some interaction between the gold nanoparticles and the DL-alanine molecules may actually take place, disturbing the alanine crystalline orientation.

In order to look for further evidence of the interaction between the gold nanoparticles and the DL-alanine molecules, FTIR spectroscopy was recorded for samples 0%npAu and 3% NpAu (Figure 5). The vibrational spectrum of DL-alanine is

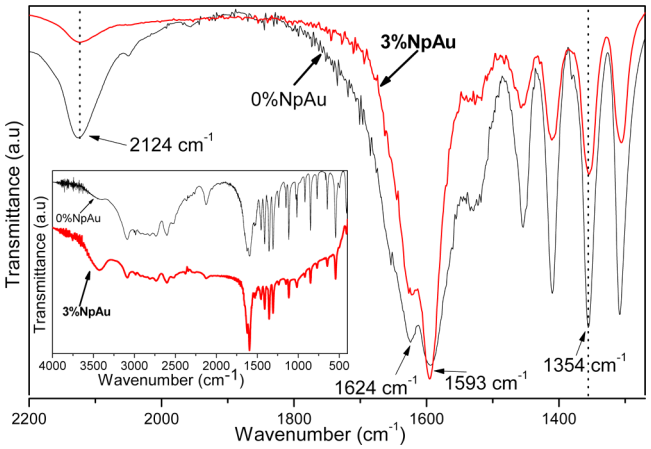

Figure 5. FTIR spectra of the nonirradiated gold/alanine nanocomposites 0%NpAu and 3%NpAu. The inset corresponds to the whole FTIR spectra of the samples (from 4000 to 400 cm^{-1}).

consistent with the characteristic FTIR spectra reported in the literature.[29,49,50] The assignments of the fundamental vibration modes due to the COO^-, NH_3^+, CH_2, C−H, C−C−N, and −OH groups are marked, and the results are summarized in Table 2.

The most significant changes in the FTIR spectra can be noted in the 2200−1300 cm^{-1} range, in the specific case of the band at 2124 cm^{-1}, associated with the combination of NH_3^+ groups symmetric stretching and bending, of the band 1624 cm^{-1}, related to the NH_3^+ asymmetric stretching group, and of the band at 1593 cm^{-1}, attributed to the asymmetric stretching of the COO^- group (Figure 5). Determination of the intensity relative to the band at 1354 cm^{-1} as an internal standard reveals a 50% reduction of the band at 2124 cm^{-1} and 20% of the band at 1624 cm^{-1}, whereas the relative intensity of the band at 1593 cm^{-1} increases 64%. The band at 1354 cm^{-1} was selected as a standard because complexes between gold and C−H radicals are not found in the literature.

Literature works have reported that the vibrational band around 2100 cm^{-1} vanishes upon formation of an alanine−copper complex.[51] Usually, amine groups do not react with gold. However, a colloidal dispersion of gold nanoparticles interacts with this group by means of weak covalent binding.[52−54] It has been described that interaction between gold nanoparticles and NH_2 occurs by means of a weak

Table 2. Assignments of the Fundamental Vibrational Modes Due to the COO^-, NH_3^+, CH_2, CH, CCN, and OH Groups of the DL-Alanine Molecules

wavenumber (cm^{-1})	assignments
544	COO^- rock
646	COO^- scissoring
770	O−C−O bending
850	C−C−N symmetric stretching
918	C−C−N symmetric stretching
1018	C−N symmetric stretching
1113	COO^- symmetric stretching
1151	COO^- symmetric stretching; NH_3^+ rock
1238	COO^- symmetric stretching
1305	COO^- symmetric stretching
1354	CH_2 wagging; CH_3 asymmetric stretching
1411	COO^- symmetric stretching
1456	CH symmetric stretching
1520	NH_3^+ symmetric stretching
1593	$NH3^+$ asymmetric stretching
1624	NH_3^+ asymmetric stretching
2124	NH_3^+ bending
2605	CH asymmetric stretching
3088	NH_3^+ symmetric stretching
3427	OH symmetric stretching

covalent binding, whereas the NH_3^+ group binds electrostatically to negative surfaces on gold nanoparticles. Because the nanocomposites always contain alanine excess compared with the amount of gold, the nanocomposites may present alanine bound and not bound to the gold nanoparticle surfaces. Thus, the reduced relative intensity of the band at 2124 cm^{-1} for the nanocomposite 3%NpAu suggests that the interaction between the gold nanoparticles and the DL-alanine molecules takes place via NH groups.

Figure 6 shows the transmission electron microscopy (TEM) images of the gold nanoparticles obtained from sample 1% NpAu. The nanoparticles are spherical and well-dispersed, as was previously pointed by UV−vis spectroscopy. Figure 6b corresponds to a magnification of the region highlighted in Figure 6a. The gold nanoparticle average size estimated by means of this figure is 9 ± 4 nm, which is close to the mean value obtained by the DLS technique. Here it is noteworthy that, although for samples with a gold mass percentage above 0.1% the XRD patterns have suggested that the exceeding nanoparticles were expelled from the alanine matrix, they seem to be stable in terms of size and no agglomeration is evident in the TEM images. This means that the nanocomposites are homogeneous even for a high gold mass percentage.

Because the influence of high-atomic-number materials is more relevant for low-energy photons, the powdered nanocomposites were irradiated with an X-ray beam with an effective energy of 90 keV and a dose of 5 Gy, in order to verify whether the interaction between the alanine molecules and the gold nanoparticles modifies the radiation-induced free-radical production. The typical ESR spectrum of the alanine radiation-induced free radicals consists of five lines because of the hyperfine interactions of the unpaired electron with four hydrogen atoms in the stable $CH_3C^{\bullet}HCOOH$ radical, named R1.[55] The relative intensities of these lines obey a 1:4:6:4:1 ratio.[16] A total of three radicals (R1, R2, and R3) is ascribed as composing the total ESR spectrum of alanine, but the R1 has been reported as the major contributor to the central electron

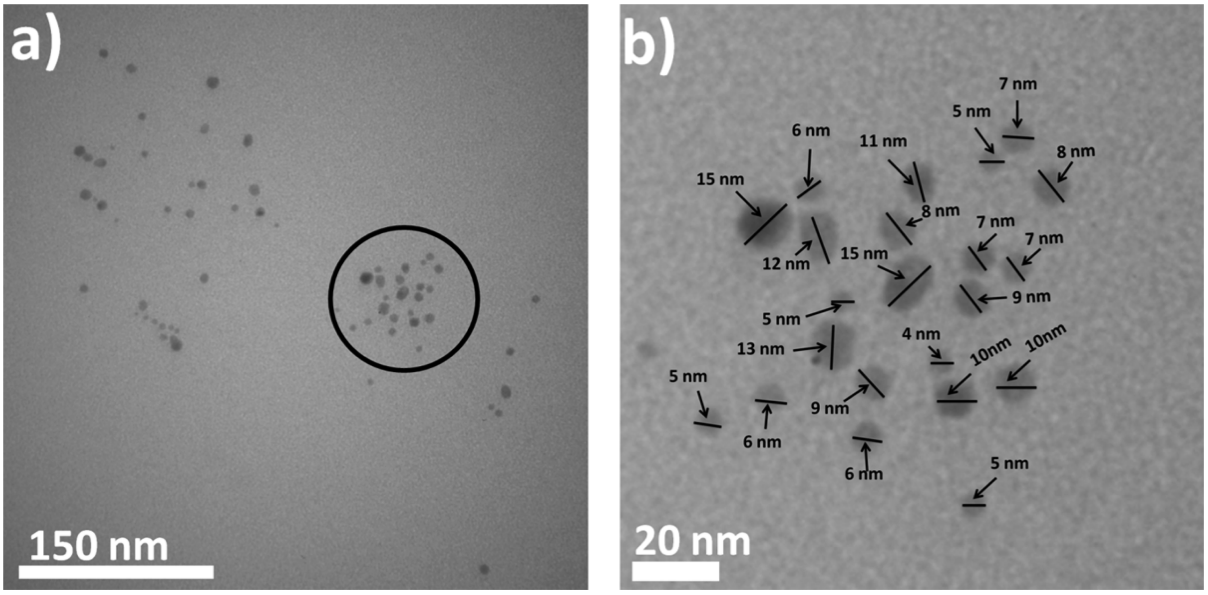

Figure 6. TEM micrographs of the sample 1%NpAu.

paramagnetic resonance line.[55] Figure 7 represents the ESR spectra registered for the irradiated samples 0%NpAu, 1%

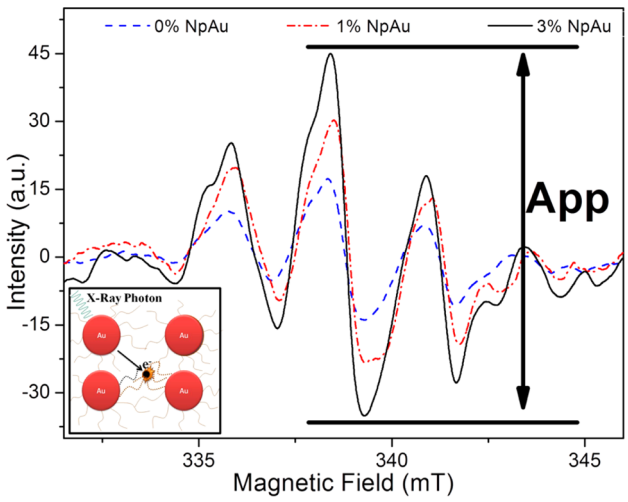

Figure 7. ESR spectra of the irradiated samples 0%NpAu, 1%NpAu, and 3%NpAu. The inset illustrates the enhancement of the number of radiation-induced free radicals caused by the interaction of the electrons ejected by the gold nanoparticles. This illustration was adapted from ref 29.

NpAu, and 3%NpAu. The relative intensity of the five lines in the ESR spectra shows that mainly the same free radical (R1) is formed in the case of gold/alanine nanocomposites. The small differences observed in the spectra of samples 1%NpAu and 3% NpAu could indicate that the production of radicals R2 and R3 is enhanced, but more detailed studies are necessary.

Figure 7 displays the ESR spectra of the irradiated samples 1%NpAg and 3%NpAg, where the intensity of the spectra of samples containing gold nanoparticles is augmented. It is well-known that the intensity of the ESR spectra is proportional to the amount of produced radiation-induced free radicals. Thus, the presence of gold nanoparticles elevated the amount of free radicals generated upon irradiation. This enhancement in free-radical production can be attributed to the high atomic number of the gold nanoparticles. The cross section for the photoelectric effect for gold atoms is larger compared to alanine, thereby increasing the amount of energy transferred to the medium and causing an increase in the production of free radicals, as schematized in the inset of Figure 7. The enhancement in the free-radical production is 1.7 ± 0.1 and 2.6 ± 0.2 for the samples 1%NpAu and 3%NpAu, respectively. This means that sample 3%NpAu is 2.6-fold more sensitive to radiation than pure DL-alanine. Here it is worth noting that these values of spectral enhancement can vary according to the energy and to the kind of radiation, besides the gold/alanine mass percentage.

In fact, the sensitivity of silver/alanine nanocomposites employed as radiation detectors can be optimized in the case of systems containing small particles (30 nm) that were well-dispersed in the alanine matrix.[29] The increase in the silver mass percentage caused agglomeration and particle growth (up to 1.5 μm), thereby diminishing the sensitivity to radiation,[29] probably by the increased self-absorption of the energy by the large particles.[37] This highlights the advantages of using gold nanoparticles instead of silver nanoparticles, which are size stability and homogeneity even for samples with high gold mass percentage. Moreover, the high atomic number of gold (Z = 79) is responsible for enhancements of the sensitivity even higher than the ones obtained by the presence of silver (Z = 47) at the same concentration. For example, the enhancement of sensitivity achieved for the silver/alanine nanocomposite containing 3% silver and irradiated under the same conditions is 1.9 ± 0.1, compared to 2.6 ± 0.2 obtained for 3%NpAu.[29] Once the cross section for the photoelectric effect is highly dependent on the beam energy, a substantial variation of the enhanced sensitivity as a function of the photon energy is expected, as observed in the case of alanine-containing silver nanoparticles.[36] Future studies will focus on the energy dependence of these gold/alanine nanocomposites.

Because variation in the amount of gold nanoparticles does not alter the particle size and because the nanocomposite remains homogeneous, it is possible to tune the desired sensor sensitivity for each specific application by easily changing the amount of gold nanoparticles in the nanocomposites, without

worrying about the influence of the nanoparticle size on radiation absorption. This is evident in Figure 8, which

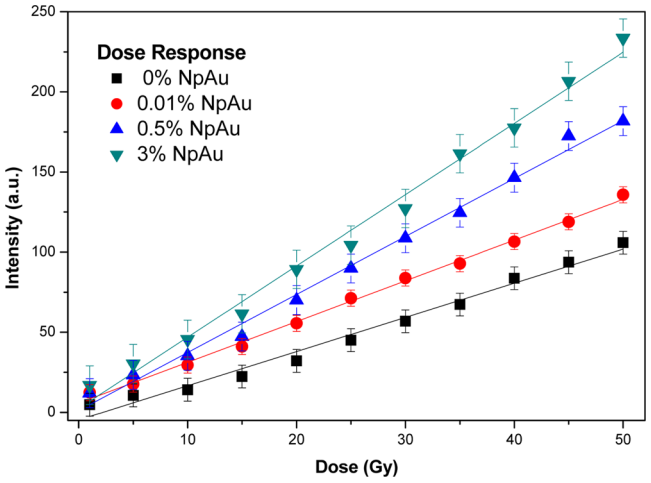

Figure 8. Intensity of the ESR spectra as a function of the doses (dose response curve) for samples 0%NpAu, 0.01%NpAu, 0.5%NpAu, and 3%NpAu. The intensity is proportional to the spin concentration per mass, and it is given in arbitrary units (au).

corresponds to the dose−response curves of the nanocomposites 0%NpAu, 0.01%NpAu, 0.5%NpAu, and 3%NpAu. The linearity typical of pure DL-alanine is not lost after the addition of gold nanoparticles. The linear, angular, and correlation coefficients are −4.7 au, 2.1 au/Gy, and *Cc* = 0.98; 5.7 au, 2.5 au/Gy, and *Cc* = 1; 1.13 au, 3.6 au/Gy, and *Cc* = 0.99; and 2.4 au, 4.5 au/Gy, and *Cc* = 0.99, respectively. Therefore, taking together the stability of the size of the nanoparticles, the good homogeneity of the nanocomposites derived from the interaction between the gold nanoparticles and the amino acid molecules, the enhanced sensitivity to radiation, and the linearity with doses, these gold/alanine nanocomposites are promising nanomaterials with tunable sensitivity for radiation dose assessment.

4. CONCLUSIONS

Gold/alanine nanocomposites containing 5-nm gold nanoparticles were synthesized, with no evidence of aggregation even for nanocomposites containing a gold mass percentage up to 3%. The addition of a small amount of gold nanoparticles culminates with the latter being accommodated inside the alanine crystals. The addition of more gold nanoparticles causes the exceeding particles to be arranged outside the alanine crystals. Interaction of the gold nanoparticles with the alanine molecules' NH group is believed to provide the nanocomposite with stability. TEM images confirmed the spherical shape of the nanoparticles, and no agglomerates were observed. The application of these nanocomposites as radiation detectors using the ESR technique revealed that the same free radical is formed in both cases of gold/alanine nanocomposites and pure alanine. The presence of gold nanoparticles in the alanine matrix resulted in enhancement of the sensitivity of such radiation sensors. Thus, these featured properties (homogeneity, size stability, and enhanced sensitivity) makes these nanocomposites potential candidates for the construction of small-sized radiation sensors with tunable sensitivity for each specific application in various medical procedures. Further studies will focus on characterization of their dosimetric properties, such as the energy dependence.

AUTHOR INFORMATION

Corresponding Author

*Tel: +55 (16) 3602-3857. E-mail: ederguidelli@pg.ffclrp.usp.br.

Notes

The authors declare no competing financial interest.

ACKNOWLEDGMENTS

This work was supported by the Brazilian funding agencies FAPESP, CNPq, and CAPES. The authors thank C. A. Brunello, E de Paula, and L. L. Amaral for technical assistance, Professor A. S. Ito for use of his UV−vis spectrometer, and Dr. Cynthia Maria de Campos Prado Manso for language revision.

REFERENCES

(1) Mack, A.; Scheib, S. G.; Major, J.; Gianolini, S.; Pazmandi, G.; Feist, H.; Czempiel, H.; Kreiner, H. J. *Med. Phys.* **2002**, *29* (9), 2080−2089.
(2) Pantelis, E.; Moutsatsos, A.; Zourari, K.; Kilby, W.; Antypas, C.; Papagiannis, P.; Karaiskos, P.; Georgiou, E.; Sakelliou, L. *Med. Phys.* **2010**, *37* (5), 2369−2379.
(3) Gruenheid, T.; Schieck, J. R. K.; Pliska, B. T.; Ahmad, M.; Larson, B. E. *Am. J. Orthod. Dentofac.* **2012**, *141* (4), 436−443.
(4) Hassouna, A. H.; Bahadur, Y. A.; Constantinescu, C.; El Sayed, M. E.; Naseem, H.; Naga, A. F. *Brachytherapy* **2011**, *10* (6), 498−502.
(5) Johnson, P. B.; Geyer, A.; Borrego, D.; Ficarrotta, K.; Johnson, K.; Bolch, W. E. *Med. Phys.* **2011**, *38* (2), 1008−1017.
(6) Agosteo, S. *Radiat. Meas.* **2010**, *45* (10), 1171−1177.
(7) Sommer, M.; Jahn, A.; Henniger, J. *Radiat. Meas.* **2011**, *46* (12), 1818−1821.
(8) Lang, S.; Hrbacek, J.; Leong, A.; Kloeck, S. *Phys. Med. Biol.* **2012**, *57* (9), NIL_457−NIL_465.
(9) Singh, M.; Kaur, N.; Singh, L. *Nucl. Instrum. Methods Phys. Res., Sect. B* **2012**, *276*, 19−24.
(10) Yukihara, E. G.; McKeever, S. W. S. *Phys. Med. Biol.* **2008**, *53* (20), R351−R379.
(11) Qi, Z.-Y.; Deng, X.-W.; Huang, S.-M.; Shiu, A.; Lerch, M.; Metcalfe, P.; Rosenfeld, A.; Kron, T. *Int. J. Radiat. Oncol.* **2011**, *80* (5), 1581−1588.
(12) Ikeya, M.; Hassan, G. M.; Sasaoka, H.; Kinoshita, Y.; Takaki, S.; Yamanaka, C. *Appl. Radiat. Isot.* **2000**, *52* (5), 1209−1215.
(13) Lund, E.; Gustafsson, H.; Danilczuk, M.; Sastry, M. D.; Lund, A.; Vestad, T. A.; Malinen, E.; Hole, E. O.; Sagstuen, E. *Appl. Radiat. Isot.* **2005**, *62* (2), 317−324.
(14) Rossi, B. T.; Chen, F.; Baffa, O. *Appl. Radiat. Isot.* **2005**, *62* (2), 287−291.
(15) Chu, S.; Wieser, A.; Feist, H.; Regulla, D. F. *Appl. Radiat. Isot.* **1989**, *40* (10−12), 993−996.
(16) Regulla, D. F.; Deffner, U. *Int. J. Appl. Radiat. Isot.* **1982**, *33* (11), 1101−&.
(17) Baffa, O.; Kinoshita, A.; Abrego, F. C.; dos Santos, A. B.; Rossi, B.; Graeff, C. *Med. Phys.* **2004**, *724*, 41−52.
(18) Miyagusku, L.; Chen, F.; Kuaye, A.; Castilho, C. J. C.; Baffa, O. *Radiat. Meas.* **2007**, *42* (6−7), 1222−1226.
(19) Chen, F.; Covas, D. T.; Baffa, O. *Appl. Radiat. Isot.* **2001**, *55* (1), 13−16.
(20) Schaeken, B.; Scalliet, P. *Appl. Radiat. Isot.* **1996**, *47* (11−12), 1177−1182.
(21) Chen, F.; Nicolucci, P.; Baffa, O. *Radiat. Meas.* **2008**, *43* (2−6), 467−470.
(22) Chen, F.; Graeff, C. F. O.; Baffa, O. *Nucl. Instrum. Methods Phys. Res., Sect. B* **2007**, *264* (2), 277−281.
(23) Abrego, F. C.; Calcina, C. S. G.; de Almeida, A.; de Almeida, C. E.; Baffa, O. *Med. Phys.* **2007**, *34* (5), 1573−1582.

(24) Brai, M.; Gennaro, G.; Marrale, M.; Bartolotta, A.; D'Oca, M. C. *Appl. Radiat. Isot.* **2007**, *65* (4), 435−439.
(25) Chen, F.; Ramirez, J. V.; Nicolucci, P.; Baffa, O. *Health Phys.* **2010**, *98* (2), 383−387.
(26) Gustafsson, H.; Danilezuk, M.; Sastry, M. D.; Lund, A.; Lund, E. *Spectrochim. Acta A* **2005**, *62* (1−3), 614−620.
(27) Brai, M.; Gennaro, G.; Marrale, M.; Tranchina, L.; Bartolotta, A.; D'Oca, M. C. *Radiat. Meas.* **2007**, *42* (2), 225−231.
(28) Hassan, G. M.; Ikeya, M. *Appl. Radiat. Isot.* **2000**, *52* (5), 1247−1254.
(29) Guidelli, E. J.; Ramos, A. P.; Zaniquelli, M. E. D.; Nicolucci, P.; Baffa, O. *Nanoscale* **2012**, *4* (9), 2884−2893.
(30) Guidelli, E. J.; Ramos, A. P.; Zaniquelli, M. E. D.; Baffa, O. *Spectrochim. Acta A* **2011**, *82* (1), 140−145.
(31) Lee, G. J.; Shin, S. I.; Kim, Y. C.; Oh, S. G. *Mater. Chem. Phys.* **2004**, *84* (2−3), 197−204.
(32) Villa-Sanchez, G.; Mendoza-Anaya, D.; Gutierrez-Wing, C.; Perez-Hernandez, R.; Gonzalez-Martinez, P. R.; Angeles-Chavez, C. *Nanotechnology* **2007**, *18*, 26.
(33) Mendoza-Anaya, D.; Angeles, C.; Salas, P.; Rodriguez, R.; Castano, V. M. *Nanotechnology* **2003**, *14* (12), L19−L22.
(34) Gao, X.; Kang, Q. S.; Yeow, J. T. W.; Barnett, R. *Nanotechnology* **2010**, *21*, 28.
(35) Marrale, M.; Longo, A.; Spano, M.; Bartolotta, A.; D'Oca, M. C.; Brai, M. *Radiat. Res.* **2011**, *176* (6), 821−826.
(36) Guidelli, E. J.; Ramos, A. P.; Zaniquelli, M. E. D.; Nicolucci, P.; Beffa, O. *Radiat. Phys. Chem.* **2012**, *81* (3), 301−307.
(37) Leung, M. K. K.; Chow, J. C. L.; Chithrani, B. D.; Lee, M. J. G.; Oms, B.; Jaffray, D. A. *Med. Phys.* **2011**, *38* (2), 624−631.
(38) Tomal, A.; Cunha, D. M.; Antoniassi, M.; Poletti, M. E. *Appl. Radiat. Isot.* **2012**, DOI:10.1016/j.apradiso.2011.11.044.
(39) Sun, H. M.; Gao, Z. W.; Gao, L. X.; Hou, K. *J. Macromol. Sci. A* **2011**, *48* (4), 291−298.
(40) Parab, H.; Jung, C.; Woo, M. A.; Park, H. G. *J. Nanopart. Res.* **2011**, *13* (5), 2173−2180.
(41) Medina-Ramirez, I.; Bashir, S.; Luo, Z. P.; Liu, J. L. *Colloid Surf. B* **2009**, *73* (2), 185−191.
(42) Rafey, A.; Shrivastavaa, K. B. L.; Iqbal, S. A.; Khan, Z. *J. Colloid Interface Sci.* **2011**, *354* (1), 190−195.
(43) Sun, Y. G.; Xia, Y. N. *Science* **2002**, *298* (5601), 2176−2179.
(44) Frens, G. *Kolloid Z. Z. Polym.* **1972**, *250* (7), 736−&.
(45) Potara, M.; Maniu, D.; Astilean, S. *Nanotechnology* **2009**, *20*, 31.
(46) Calvin, S.; Luo, S. X.; Caragianis-Broadbridge, C.; McGuinness, J. K.; Anderson, E.; Lehman, A.; Wee, K. H.; Morrison, S. A.; Kurihara, L. K. *Appl. Phys. Lett.* **2005**, *87*, 23.
(47) Li, T. H.; Park, H. G.; Lee, H. S.; Choi, S. H. *Nanotechnology* **2004**, *15* (10), S660−S663.
(48) Koyama, M.; Shiraishi, M.; Sasaki, K.; Kon-no, K. *J. Dispersion Sci. Technol.* **2008**, *29* (9), 1266−1271.
(49) Caroline, M. L.; Sankar, R.; Indirani, R. M.; Vasudevan, S. *Mater. Chem. Phys.* **2009**, *114* (1), 490−494.
(50) Jaikumar, D.; Kalainathan, S.; Bhagavanarayana, G. *J. Cryst. Growth* **2009**, *312* (1), 120−124.
(51) Tarallo, M. B.; Costa-Filho, A. J.; Vieira, E. D.; Monge, A.; Leite, C. Q.; Borthagaray, G.; Gambino, D.; Torre, M. H. *An. Asoc. Quím. Argent.* **2009**, *97*, 9.
(52) Leff, D. V.; Brandt, L.; Heath, J. R. *Langmuir* **1996**, *12* (20), 4723−4730.
(53) Kumar, A.; Mandal, S.; Selvakannan, P. R.; Pasricha, R.; Mandale, A. B.; Sastry, M. *Langmuir* **2003**, *19* (15), 6277−6282.
(54) Sylvestre, J. P.; Poulin, S.; Kabashin, A. V.; Sacher, E.; Meunier, M.; Luong, J. H. T. *J. Phys. Chem. B* **2004**, *108* (43), 16864−16869.
(55) Malinen, E.; Hult, E. A.; Hole, E. O.; Sagstuen, E. *Radiat. Res.* **2003**, *159* (2), 149−153.